Molecular Simulations of the Imidization of Adsorbed Polyamic Acid

J. A. Young*,†

Department of Materials Science and Engineering, University of Virginia, Charlottesville, Virginia 22903

J. A. Hinkley

Materials Division, NASA Langley Research Center, Hampton, Virginia 23681

B. L. Farmer‡

Department of Materials Science and Engineering, University of Virginia, Charlottesville, Virginia 22903

Received September 28, 1999; Revised Manuscript Received April 17, 2000

ABSTRACT: Computer simulations have been developed to investigate the intramolecular cyclization of polyimides (i.e., imidization, the conversion of the precursor polyamic acid into polyimide). Imidization was examined as a function of time, temperature, and presence or absence of a silica substrate. To do this, the essential results of quantum mechanical studies were incorporated into a molecular dynamics simulation. Molecular dynamics simulations were used to determine the conformational properties of the polymer chain and to simulate the imidization reaction when the conformational criteria established by quantum mechanical methods were met. In agreement with experiments, imidization occurred in two distinct stages, and increased temperatures were shown to produce higher extents of imidization. Finally, the interfacial chains exhibited more complete imidization than the isolated chains. These results not only support the proposed molecular rationale behind the kinetic models of imidization but also demonstrate that only local chain motions are necessary for imidization to occur.

Introduction

Polymer/substrate interfaces are important in determining the properties of many materials used in high-tech applications. Interfacial properties are intimately related to the macroscopic properties of the polymer/substrate system, such as moisture adsorption, adhesion, dielectric constant, failure mechanisms, and coefficient of thermal expansion.[1] Thermal stability (i.e., $T_g \approx 600$ K) along with good electrical insulation integrity, chemical stability, high mechanical strength, and low dielectric constant has made polyimides and polyimide/substrate systems a vital part of many technologies.

To fully understand the polyimide/substrate interface, it is necessary to examine the two-stage synthesis by which such systems are prepared. Polyamic acid (PAA) is first synthesized and cast onto the substrate. Thermal imidization at temperatures ranging from 300 to 700 K then follows. As imidization proceeds, the polymer undergoes intramolecular cyclization, causing continuous changes in the material properties.[2−5] Because interfacial properties greatly influence the durability and performance of polyimide-based microelectronic and composite systems, the final extent of imidization near the interface is of considerable interest.

Solid-state thermal imidization is not well understood due to the presence of a multitude of variables including residual solvent, hydrogen bonding between polar solvents and the polymer, film thickness, and molecular mobility.[6] While the lack of solubility of polyimides prevents a detailed and comprehensive experimental evaluation of the molecular mechanisms of imidization, methods such as FTIR and NMR are capable of tracking the overall imidization process. It has been found that imidization occurs in two stages, the first being one of rapid cyclization followed by a period of slower cyclization. To explain the experimental data, two kinetic models have been proposed: the cage theory[7] and the variable parameter theory.[8] These models are very similar in that they employ two first-order rate equations to fit the experimental data.

$$k_c = B_0 \exp(-E/RT) \tag{1}$$

$$k_j = A_0 f(j) \exp(-U/RT) \tag{2}$$

The variables are afforded the following physical meanings: k_c is the chemical rate constant which describes the chemical conversion of an amic acid group into imide. k_j describes the process by which amic acid groups undergo conformational transformations between nonequivalent conformational states to align these groups for imidization. A_0 and B_0 are the preexponentials of the activation entropies for transition between states and for the reaction of ring closure, respectively. $f(j)$ is a decreasing function of time (i.e., increasing extent of imidization) which is attributed to both the decrease in the number of unreacted sites and the loss of a degree of freedom due to ring closure. The specific form of this function differs in the cage and variable parameter models.[7,8] E and U are the activation energies of the chemical reaction and the entropy, respectively. The physical reasoning behind the two-stage kinetic models is as follows. Initially, the PAA contains a portion of the functional groups in position for imidization. In the first stage of imidization it is the chemical conversion of these amic acid groups into

† Present address: Lawrence Livermore National Laboratory, L 474, Livermore, CA 94550-9234.

‡ Present address: Air Force Research Laboratory, AFRL/MLBP, 2941 P Street, Suit 1, Wright-Patterson Airforce Base, OH 45433-7750.

10.1021/ma991639u CCC: $19.00
Published on Web 06/09/2000

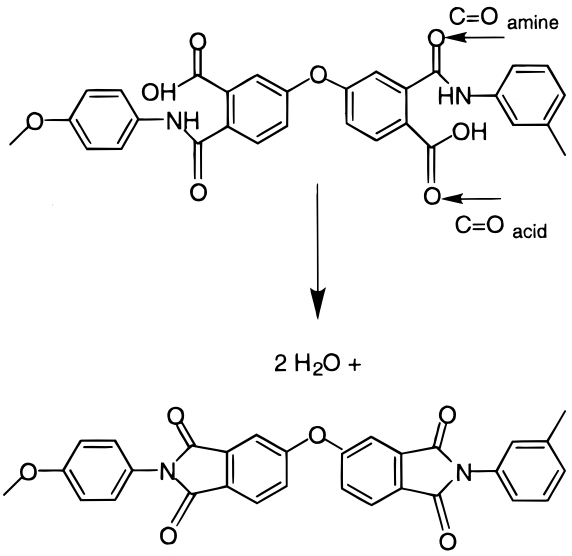

Figure 1. Imidization of LaRC-IA polyamic acid (PAA) into polyimide. Relevant chemical moieties are noted.

polyimide, k_c, which is rate-determining. In the second stage, the ability of the functional groups to move between nonequivalent conformational states is rate-determining. The computer simulation presented in this paper examines in detail the proposed physical characteristics underlying the kinetic models of imidization.

The challenge of modeling polyimide interfaces lies in the fact that both the polymer/substrate interactions and the chemical reaction of imidization must be modeled. Previously, Monte Carlo[9,10] and molecular dynamics[11−13] techniques have been applied to bulk polymers near interfaces. Although the molecular dynamics method provides an effective and efficient tool for examining the conformational properties of polymer chains, it is unable to simulate chemical reactions within the system. Quantum mechanical methods are necessary to examine chemical reactions. Although simultaneous quantum/molecular mechanical methods are being developed,[14,15] they remain quite computationally time-consuming even for simple systems.

This paper presents an atomistic simulation of the imidization of 4,4′-oxydiphthalic dianhydride/3,4′-oxydianiline (LaRC-IA) polyimide (see Figure 1). Imidization is simulated as a function of time and temperature. The results are related to the kinetic models outlined above. Finally, interfacial imidization is examined by comparing the imidization of isolated chains to chains in the vicinity of a fully hydroxylated silica substrate.

Method

This work seeks to map the essential features of quantum mechanical studies of imidization into a molecular dynamics simulation for the purpose of gaining a better understanding of the imidization process. Quantum mechanics was used to develop a force field and establish conformational criteria for imidization. Molecular dynamics was then employed to examine the motions of the polymer chain before, during, and after imidization. This combination of quantum and classical calculations lends valuable insights into both the chemistry and chain dynamics of imidization.

Force Field. The usefulness of a classical molecular dynamics simulation depends largely on the quality of the underlying force field. The CFF91 force field[16] within the BIOSYM Molecular Modeling software was modified to accurately describe the conformational properties of the LaRC-IA polyamic acid. The modified CFF91 force field was obtained by altering selected parameters such that the resulting potential energy surfaces of appropriate model compounds agreed with those obtained by quantum mechanical methods. Figure 2 shows the torsional rotations, angle bends, and the associated atom potentials that had to be parametrized. The functional form of the torsional barrier is a three-term Fourier expansion:

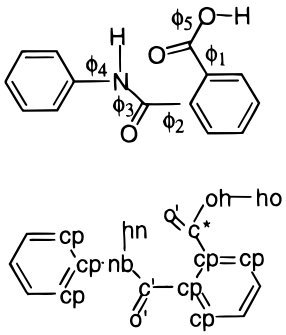

Figure 2. Torsions and atomic potential types for the parametrization of PAA.

$$E_{\text{torsion}} = K_1(1 - \cos(\phi - \phi_1^0)) + K_2(1 - \cos(\phi - \phi_2^0)) + K_3(1 - \cos(\phi - \phi_3^0)) \quad (3)$$

The angle bending term is a quartic polynomial:

$$E_{\text{angle}} = H_2(\theta - \theta^0)^2 + H_3(\theta - \theta^0)^3 + H_4(\theta - \theta^0)^4 \quad (4)$$

K_i and H_i are the parameters of the force field and ϕ_i^0 and θ^0 are the equilibrium values of the torsions and bond angles, respectively. NMR, ab initio, and semiempirical results were used to parametrize the following torsions: the amide torsion (ϕ_3 of Figure 2),[17] the diamine ring torsion[18] (ϕ_4 of Figure 2), the dianhydride backbone ring torsion[18] (ϕ_2 of Figure 2), and the carboxyl torsion[19] (ϕ_1 of Figure 2). The acid torsion (ϕ_5 of Figure 2) was not available in the literature and therefore was determined using the AM1 Hamiltonian within MOPAC.[20] Table 1a,b summarizes the altered force field parameters that comprise the modified CFF91 force field. Partial atomic charges were taken from semiempirical quantum mechanical calculations using AM1 on the LaRC-IA polyamic acid and the imidized LaRC-IA.

Imidization Criteria. Previous quantum mechanical calculations have examined the transition states involved in the transformation of polyamic acid into polyimide.[7,21−23] Imidization is believed to occur via the formation of neutral tetrahedral intermediate states for which there are two possible pathways (see Figure 3). The calculated energy barrier for the synchronous substitution mechanism (S_N2) is an order of magnitude higher than that for the addition−elimination (AE) pathway.[21,24] Therefore, the AE mechanism is the most probable reaction path. It involves a tetrahedral intermediate, INT, which requires the simultaneous formation of a C−N bond and proton transfer from the amide nitrogen to the carbonyl oxygen.

Unfortunately, there are no published data regarding the specific geometries of these transition states. Therefore, calculations were carried out to determine conformational criteria for imidization, specifically, the align-

Table 1. Force Field Parameters for LaRC-IA Polyamic Acid[a]

a. Torsional Force Field Parameters for LaRC-IA Polyamic Acid[b]

atom 1	atom 2	atom 3	atom 4	K_1	K_2	K_3
O′	C*	CP	CP	0	0.5000	0
OH	C*	CP	CP	0	0.5000	0
CP	CP	NB	C′	0	0.6600	0
HN	NB	CP	CP	0	0.6600	0
CP	CP	C′	NB	0	0.2600	0
CP	CP	C′	O′	0	0.2600	0
HC	CP	CP	C*	0	1.3000	0
C*	CP	CP	C′	0	5.3000	0
C*	CP	CP	CP	0	5.3000	0
HC	CP	CP	C′	0	1.3000	0
HO	OH	C*	CP	−2.7332	2.9646	−0.0155
CP	NB	C′	CP	.7000	5.3000	0
HN	NB	C′	O′	.7000	5.3000	0
HN	NB	C′	CP	.7000	5.3000	0
O′	C′	NB	CP	.7000	5.3000	0
C′	NB	CP	CP	−0.1047	.2465	−0.0234

b. Angle Bending Force Field Parameters for LaRC-IA Polyamic Acid[c]

atom 1	atom 2	atom 3	H_2	θ_0 (deg)
cp	c*	o′	68	126
c′	nb	cp	50	126
c′	nb	h*	35	117

[a] K_1, K_2, K_3, and H_2 are in kcal/mol. [b] $\phi_1^0 = \phi_2^0 = \phi_3^0 = 0°$ [c] See Figure 2. $H_1 = H_3 = 0$ kcal/mol.

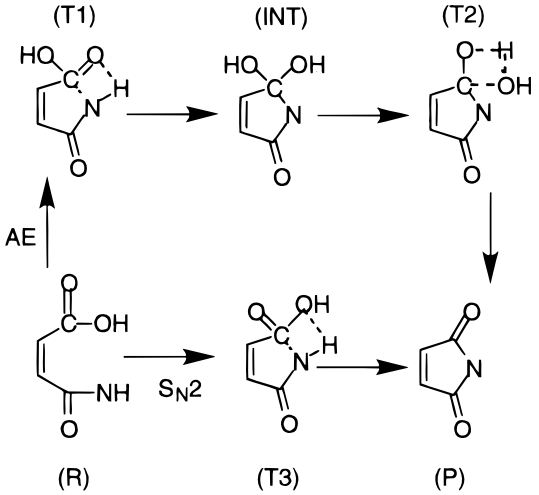

Figure 3. Neutral transition states in the transformation of PAA (R) into polyimide (P). AE and S_N2 pathways are shown. Dotted lines represent hydrogen bonding and partial covalent bonds.

ment of the COOH and CONH functional groups which lead to the formation of the INT intermediate state. This was accomplished by scanning the carboxyl, ϕ_1, and dianhydride backbone torsions, ϕ_2, of the *N*-phenylphthalic acid model compound (see Figure 2). As these groups were rotated, the remainder of the molecule was allowed to relax. This procedure was done both quantum mechanically using the AM1 Hamilitonian within MOPAC and classically using the modified CFF91 force field.

The conformations likely to form the INT neutral tetrahedral intermediate were selected by focusing on the simultaneous formation of the C−N bond and transfer of the amide hydrogen to the double-bonded oxygen of the carboxylic acid. A contour plot of the C−N separation distance as a function of conformation reveals one broad minimum region spanning the majority

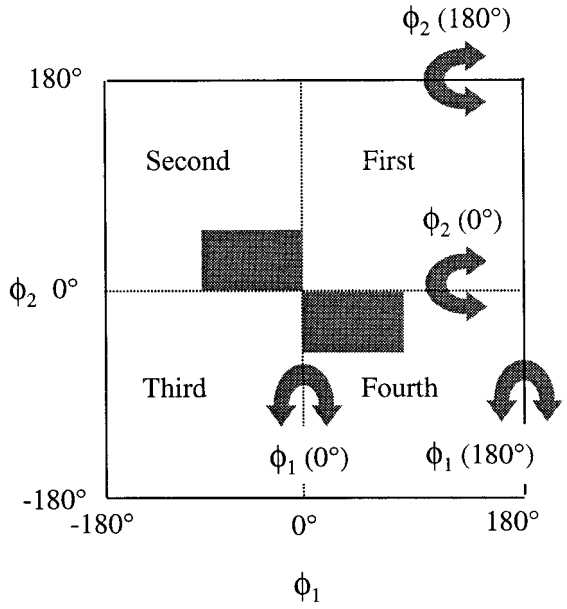

Figure 4. Quadrants as defined by the carboxyl and dianhydride backbone torsions. Torsional transitions are labeled and indicated by arrows. The conformational regions that meet the imidization criteria are shaded.

of the carboxyl, ϕ_1, torsions. The separation distance between the amide hydrogen and the double-bonded oxygen of the carboxylic acid has two symmetric minima, in the second and fourth quadrants. It is these conformations which facilitate proton transfer to the carboxyl group and formation of the tetrahedral intermediate. For these simulations, imidization was therefore defined to occur when $-90° < \phi_1 < 0°$ and $0° < \phi_2 < 45°$ or $0° < \phi_1 < 90°$ and $-45° < \phi_2 < 0°$ (see Figure 4). These criteria mean that only 6% of the conformational space covered by these torsions leads to imidization.

In the molecular dynamics simulations, once one amic acid group of the chain reached a conformation in accord with these criteria, imidization of that segment was forced to occur instantaneously. The transition through the INT, T1, and T2 intermediate states was not modeled. The chain transformed directly from the polyamic acid into polyimide and water. The ab initio calculations necessary to further refine the imidization criteria, to describe the exact geometry and electron distributions in the transition states, and to obtain a rate constant for the reaction were beyond the scope of the present work.

Calculations also revealed that the global energy minima for this model compound lie in the second and forth quadrants near the previously defined imidizable conformations. There also exist local energy minima in the first and third quadrants whose conformations resemble the T3 intermediate. The arrows in Figure 4 illustrate the transitions between the quadrants. By symmetry, the first and third quadrants are equivalent, as are the second and fourth.

Silica Surface. Interfacial properties are largely determined by the choice of polymer and substrate. The deposition of PAA onto a silicon substrate covered by oxide layers of silica, SiO_2, has considerable industrial importance. SiO_2 is an acidic substrate having an isoelectric point of the surface (IEPS) value of 2.2 (IEPS = 5.0 indicates a neutral surface).[25] Due to the acidic nature of both the substrate and the PAA, only weak interactions indicative of physisorption are expected.

Table 2. ΔH as a Function of Dielectric Constant for Model Compounds on the Silica Substrate; All Energies Are in kcal/mol

	isolated energy	ΔH ($\epsilon = 1$)	internal energy ($\epsilon = 1$)	ΔH ($\epsilon = 15$)	internal energy ($\epsilon = 15$)	ΔH (literature)
benzene	1	−139	15	−13	1	−5 to −13 (ref 42)
methoxy	−2	−71	0	−12	−2	−14 to −16 (ref 28)
water	0	−150	31	−11	0	−4 to −11 (ref 28)

This is confirmed by experimental studies which show that polyamic acid does not chemically react with native silicon oxide surfaces.[26,27]

The (111) surface of cristobalite silica was chosen as the model of the SiO_2 substrate. The following procedure was employed to build the surface. The CERIUS molecular modeling package was used to build the cristobalite tetrahedral crystal structure. The crystal was cleaved along the (111) plane, and hydroxyl groups were added to the surface to fill dangling bonds. The result was an 80 Å × 9 Å × 60 Å fully hydroxylated silica substrate in which the $x-z$ plane defines the surface of the substrate.

Electrostatic interactions between the substrate and adsorbate strongly affect the energetics and conformations of the adsorbate during physisorption. The electrostatic interactions were computed as $(q_i q_j)/(\epsilon r_{ij})$ where q_i and q_j are the partial atomic charges, r_{ij} is the distance separating the two atoms, and ϵ is the dielectric constant of the system. Unfortunately, no reliable quantum mechanical method exists for the accurate assignment of charges to the substrate. When models of the silica surface have been needed, most authors have used cluster or embedded cluster techniques.[28] These methods tend to underestimate the acidity of the surface OH groups,[29] and the charges are dependent upon the size of the cluster used.[28] When molecular dynamics have been used to investigate interfaces, various strategies for dealing with the electrostatic problem have been employed: the ad hoc addition of acidity parameters,[30] the scaling of substrate charges,[31] and the use of an external potential.[32] In all cases, the necessary parameters were obtained by fitting to experimental adsorption data. The dielectric constant most drastically affects the substrate/adsorbate binding energies. Therefore, for the purposes of this work, it was expedient to obtain fits to experimental data by adjusting the dielectric constant.

The partial charges on the substrate atoms were obtained from ab initio calculations[33] and adjusted to give a charge neutral substrate. The silicon atoms were assigned 1.370 e^-, the embedded oxygen atoms −0.685 e^-, the surface oxygen of the OH groups −0.767 e^-, and the surface hydrogens 0.424 e^-. Table 2 demonstrates the effect that the dielectric constant has on the internal energy and the binding energy, ΔH, of several adsorbates. It was found that inordinately large binding energies and unrealistic conformational distortions of the adsorbate result when $\epsilon = 1$, its vacuum value. Therefore, an increased value of $\epsilon = 15$ was used to dampen the electrostatic interactions. This gave the correct binding energies and conformations for a selection of model compounds on the silica surface.

The structure of the SiO_2 substrate was held motionless, and the charges of both the adsorbing species and the surface were kept constant during the simulations. The justifications for constructing the model in this manner are as follows. The structural and dynamical properties of the adsorbate are not significantly altered when substrate dynamics are omitted.[32,34] Freely rotating OH groups on the silica surface may change the acidity of the substrate surface[28] via the formation of intramolecular hydrogen bonding among surface OH groups. Finally, fixing the positions of the substrate atoms during molecular dynamics greatly reduces the computation time. In physisorbed systems such as this, the polymer and substrate interact solely through nonbonded interactions and excluded-volume considerations. The modeling of chemisorbed systems would require the examination of chemical reactions between the polymer and substrate.

Imidization Simulation. The imidization of LaRC-IA polyamic acid chains in isolation and in proximity to the silica substrate was examined. A 0.5:0.5 alternating mixture of para- and meta-isomeric monomers[21] was used to build polymer chains 10 repeat units long. This allowed 20 potential imidization sites to be monitored. Six such chains were built: three to be examined in isolation and three near the substrate. Molecular dynamics were conducted in three phases. First the behavior of the polyamic acid was examined, second the imidization was modeled, and finally the behavior of the resulting polyimide was studied.

A computer program for the simulation of the imidization reaction was written using the BIOSYM TCL (BTCL) language syntax. The program monitored the torsion angles central to imidization, ϕ_1 and ϕ_2, and performed the necessary "reaction" (i.e., changes in molecular bonding and charge assignment) when the previously stated criteria were met. The input consisted solely of the force field, the polymer chain (atom potential type, atomic charge, chain conformation, connectivity, etc.), and the simulation temperature. The LaRC-IA polyamic acid was first subjected to 100 ps of regular molecular dynamics to examine the structure and dynamics of the unimidized PAA chains. The imidization checking procedure was then activated. This subroutine periodically checked the carboxyl and dianhydride backbone torsions of all potential imidization sites. If the prescribed imidization criteria were met at a given site, then the imidization procedure was invoked. This redefined the structure of the polymer chain: the carbon−nitrogen bond was created to cyclize the imide ring, and the appropriate bonds were broken/created to form a molecule of water. Partial atomic charges and atom potential types were reassigned to reflect the formation of the imide ring and water. A brief molecular mechanics minimization was used to refine the resulting high-energy structure. A 10 fs period of molecular dynamics was used to reestablish the atomic velocities. Molecular dynamics continued for 5 fs, after which time the imidization checking procedure was again invoked. If the criteria for imidization were not met, molecular dynamics continued for 5 fs using the atomic positions, velocities, and accelerations from the previous step. This procedure continued until a total of 200 ps of imidization molecular dynamics was run.

Results

The molecular dynamics program was used to examine the PAA and the imidization of LaRC-IA as an

isolated chain and near a silica substrate at 400 and 700 K. These temperatures represent the low and high ends of the experimentally used cure temperatures.[35] The following section presents the effects that the substrate has on the overall chain dimensions of the PAA. The results of the imidization process follows.

Chain Properties. The PAA was placed on the silica surface such that the center of mass of the polymer was 6 Å above the substrate surface. During the initial 25 ps of the 100 ps molecular dynamics simulation, the PAA polymer arranged itself in a manner that reduced the total energy of the system by reduction of the polymer/substrate nonbonded energy. The average internal energy of the interfacial chains was 1330 kcal/mol (standard deviation, 39 kcal/mol), only slightly higher than that of the isolated chains 1316 kcal/mol (standard deviation, 40 kcal/mol). This indicates that although the strength of interaction between the polymer and substrate (−453 kcal/mol) was large enough to cause adsorption of the polymer, the interactions did not cause gross distortions of the conformations of the PAA chain.

PAA conformations prior to imidization were characterized by calculating the population density of each quadrant. For the isolated chains, 65% of the conformations were initially in an imidizable quadrant (i.e., the second or fourth quadrants). This is not surprising because as stated earlier, these conformations are most favorable energetically. In contrast, only 35% of the potential imidization sites in the interfacial chains occupied imidizable quadrants. This distribution of conformations may be understood by examining the orientation of these conformations with respect to the silica substrate. The orientation of the polyamic acid polar groups, C═O_{amine} and C═O_{acid}, seen in Figure 1, was examined by looking at the average angle that these groups make with each of the coordinate directions (i.e., $\langle\theta\rangle = 90°$ indicates random orientation). Both groups were randomly oriented in the plane of the substrate, the $x-z$ plane. In the y direction, these groups showed a slight preferential orientation toward the substrate, $\langle\theta_y\rangle = 115°$ and $\langle\theta_y\rangle = 104°$ for the amine and acid groups, respectively. This allows favorable electrostatic interactions between the positively charged surface hydrogen atoms of the silica (0.424 e^-) and the negatively charged oxygen atoms (−0.331 e^-) of the C═O_{amine} group. Conformations in which the C═O_{amine} and C═O_{acid} groups point in the same direction reside in the nonimidizable quadrants. This surface interaction explains the decrease in the population of conformations initially in imidizable quadrants.

Figure 5a shows the polyamic acid/silica system at the completion of the initial 100 ps molecular dynamics simulation. The overall shape of the polyamic acid chain in the presence of the substrate was examined by calculating the components of the radius of gyration, $R_{g,i}$, in each of the coordinate directions (x, y, z):

$$R_{g,i} = \left\langle \frac{1}{n_a}\sum_{j=1}^{n_a}(r_{i,j} - r_{cm,i})^2 \right\rangle \qquad (5)$$

n_a is the number of atoms in the system, $r_{i,j}$ represents the vector position (i.e., x, y, z) of the jth atom of the system, and $r_{cm,i}$ is the vector position of the center of mass of the chain. Table 3 gives the time-averaged radius of gyrations. In vacuum the chain adopts essentially spherical symmetry as evidenced by the components of the radius of gyration and as shown in Figure 5b. The presence of the silica substrate causes the chains to adapt flattened, nearly two-dimensional structures. Table 3 shows that the radius of gyration in the direction perpendicular to the substrate surface, $R_{g,y}$, decreases by approximately 75% while the total radius of gyration increases by 40%. Not surprisingly, these values obtained for single chains are consistently larger than those obtained in other studies which use

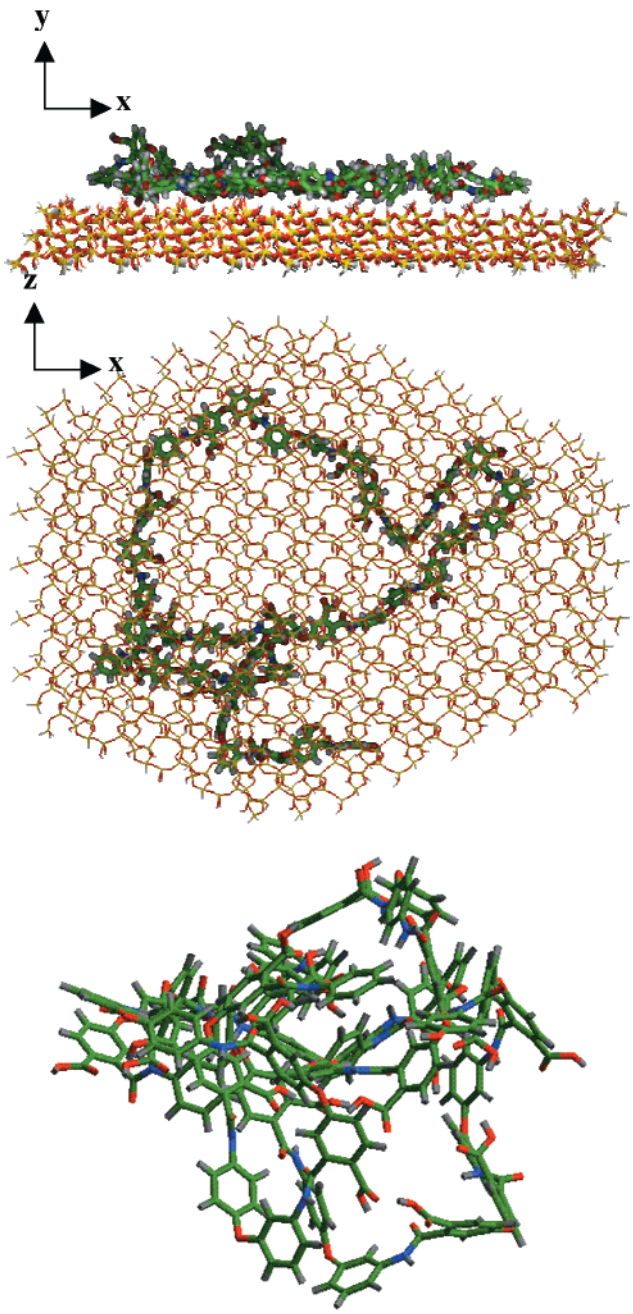

Figure 5. (a) Side and top views of the LaRC-IA/silica system. (b) Isolated LaRC-IA polyamic acid chain.

Table 3. Components of the Radius of Gyration (in Å) and Standard Deviations for Isolated and Interfacial Chains; Averages Are Taken from the Final 10 ps of the Initial 100 ps of Molecular Dynamics

	$\langle R_{g,x}^2\rangle^{1/2}$	$\langle R_{g,y}^2\rangle^{1/2}$	$\langle R_{g,z}^2\rangle^{1/2}$	$\langle R_g^2\rangle^{1/2}$
isolated chain	6.81	7.45	8.30	13.35
	(1.34)	(3.25)	(0.86)	(1.39)
chain near silica	15.07	1.85	11.91	19.32
	(1.78)	(0.24)	(1.63)	(1.35)

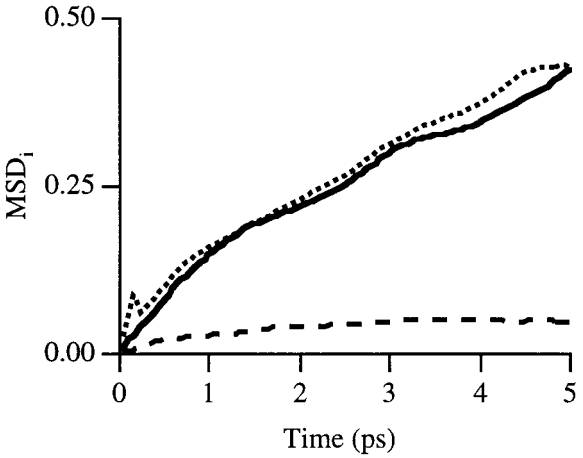

Figure 6. Components of the mean-squared displacement of the center of mass, MSD_x (dotted line), MSD_y (dashed line), and MSD_z (solid line), for interfacial PAA chains.

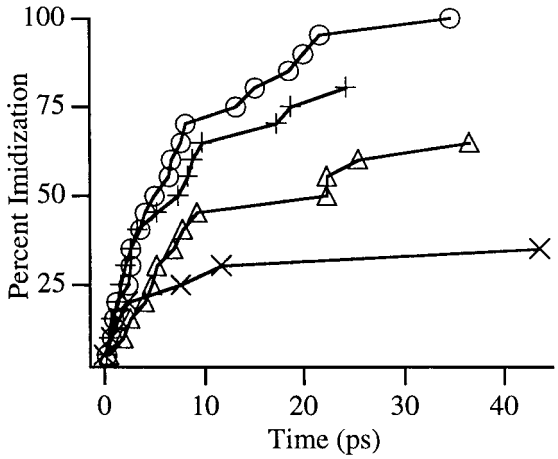

Figure 7. Extent of imidization as a function of time. Each case represents the average of three chains: (○) interfacial chains, $T = 700$ K; (△) interfacial chains, $T = 400$ K; (+) isolated chains, $T = 700$ K; and (×) isolated chains, $T = 400$ K.

multiple chains to model the full polymer melt interphase ($R_{g,y}$ decreases by 66% and R_g increases by 20%[11−13]). Experimental results also show systematic increases in the radius of gyration as the thickness of the film decreases.[36] Specifically, increases in the radius of gyration of up to 40% have been shown for films 100 Å thick. This information supports the use of a single chain model to examine the behavior of interfacial polymer chains.

In addition to the large values of $R_{g,x}$ and $R_{g,z}$, the extended nature of the interfacial chains is evidenced by both visual inspection and by the end-to-end distance of each of the monomers within the chain. The average monomer end-to-end distance in the isolated chains was 13.79 Å while that of the interfacial chains was 17.63 Å. This increase reflects the extended nature of the polymer chain when it is associated with the silica substrate.

The dynamics of the interfacial chains were also investigated. The components of the diffusion coefficient of the chain center of mass, D_x, D_y, and D_z, were examined. The components of the mean-square displacement of the center of mass of the polymer chain, MSD_x, MSD_y, and MSD_z, were first calculated.

$$\mathrm{MSD}_i = \langle [r_{\mathrm{cm},i}(t_0 + t) - r_{\mathrm{cm},i}(t)]^2 \rangle \qquad (6)$$

$r_{\mathrm{cm},i}$ is the ith component of the center of mass of the chain and t is the time. Figure 6 shows the anisotropy in the mean-squared displacement of the center of mass as a function of time. The components of the self-diffusion coefficients are easily calculated using the following equation:

$$D_i = \frac{1}{6t_c}\langle [r_{\mathrm{cm},i}(t_0 + t) - r_{\mathrm{cm},i}(t)]^2 \rangle \qquad (7)$$

The characteristic time, t_c, was taken to be 1.5 ps.[11,12] The components of the average diffusivities of the interfacial chains are $D_x = 0.126$ Å/ps, $D_y = 0.033$ Å/ps, and $D_z = 0.144$ Å/ps. Highly anisotropic chain mobility in the vicinity of the substrate is seen. Specifically, the diffusive motion of the chain is approximately 4 times faster in the transverse (x and z) directions than in the direction perpendicular the surface (y). This ratio is consistent with Monte Carlo and molecular dynamics results.[9,11−13] The (111) plane of the model surface has a topology which consists of valleys about 1 Å deep and 8.5 Å wide running parallel to the z axis. Statistically, the diffusivities and radius of gyrations in the x and z directions are similar, thus indicating that the surface topology does not significantly affect the overall mobility or shape of the chain. Other authors have reached similar conclusions.[9] The ability of this single chain model to capture both the static and dynamic properties of interfacial chains as seen in full-density models[9,11−13] and experiments[36] makes it a promising tool to investigate interfacial imidization.

Imidization. Figure 7 shows the computed extent of imidization as a function of time for all of the cases examined in this work. Each curve represents the average of three runs, each with a different starting conformation. All reactions occurred within the initial 50 ps of the 200 ps imidization simulation. Experimentally, the final extent of imidization is known to be a function of imidization temperature, higher temperatures yielding more complete imidization. The results of the simulations are consistent with this trend. In isolated chains, average extents of imidization of 35% at 400 K and 80% at 700 K were observed. The interfacial chains were 60% and 95% imidized at 400 and 700 K, respectively. It is important to note that the interfacial chains were more fully imidized than their isolated counterparts at a given temperature. Although detailed experimental investigations of interfacial imidization are difficult, evidence of complete interfacial imidization in physisorbed systems does exist, including polyimide on silica or graphite.[26,37] Finally, the shapes of the imidization curves are of importance. These curves exhibit the two-stage imidization process seen experimentally. The time scales of the processes are not comparable with those seen experimentally due to a variety of factors: the relatively broad definition of the chemical reaction of imidization, the lack of a chemical activation energy once the amic acid group has achieved the imidizable conformation, the lack of solvent in the simulation, and the examination of single chains as opposed to bulk systems. Yet as the following section will demonstrate, much can be learned about the imidization process and the role of a silica substrate.

Table 4. Number and Type of Torsional Transitions That Precede Imidization under the Four Conditions Studied in This Paper[a]

	no transition	ϕ_1	ϕ_2	total transitions
$T = 400$ K, isolated chain	21	0	0	0
$T = 700$ K, isolated chain	33	16	1	17
$T = 400$ K, interfacial chain	19	16	4	20
$T = 700$ K, interfacial chain	19	53	15	68

[a] Note that the number of ϕ_1 transitions reflects motions across both the 0° and 180° energy barriers, likewise for ϕ_2.

Discussion

To study the PAA conformations prior to imidization, the evolutions of the carboxyl, ϕ_1, and dianhydride backbone torsions, ϕ_2, were followed for each of the potential imidization sites. Torsional transitions were defined as the movement from one quadrant to another (see Figure 4). Two mechanisms of imidization are possible. If the active site initially lies in an imidizable quadrant, imidization may occur without any change of conformational state. On the other hand, transitions between states via torsional transitions may occur and sometimes lead to imidization.

Table 4 summarizes the number of reactions that occur with and without conformational transitions. As expected, there are more transitions about the freely rotating carboxyl group than the dianhydride backbone torsion. In the end the extent of imidization is limited by the ability of the system to move between the nonequivalent conformational states.

The interfacial chains are seen to exhibit a larger number of torsional transitions and higher extent of imidization (see Table 4). To examine this in detail, the first-order rotational time correlation function, $m_1(t)$, was calculated for both isolated and interfacial chains.

$$m_1(t) = \langle u(t_0)\, u(t_0 + t) \rangle \tag{8}$$

where $\mathbf{u}(t)$ is the unit vector characterizing the orientation of a bond at time t. $\mathbf{m}(t)$ was calculated for each of the bond vectors that are central to torsions ϕ_1, ϕ_2, ϕ_3, and ϕ_4 of Figure 2. The last 50 ps of the initial stage of molecular dynamics (i.e., prior to activation of the imidization procedure) was used to collect the necessary data. Figure 8 compares the rotational time correlation functions of one of the vectors, ϕ_3, for the isolated and interfacial systems. All such vectors of all three chains exhibited similar behavior. The curves do not approach the limiting value of zero due to the limitation imposed on **u** by the connectivity along the polymer backbone. For all of the polymer vectors of interest, the interfacial chains exhibit faster decay times than the isolated chains. The lower values of $m_1(t)$ arise from larger amplitudes of the torsional oscillations in the interfacial polyamic acid chains. The decreased relaxation times exhibited by the interfacial chains indicate that one of the effects of the substrate is to promote local torsional mobility at the PAA active sites. Increased local chain motions in turn result in larger extents of imidization in the LaRC-IA interfacial chains.

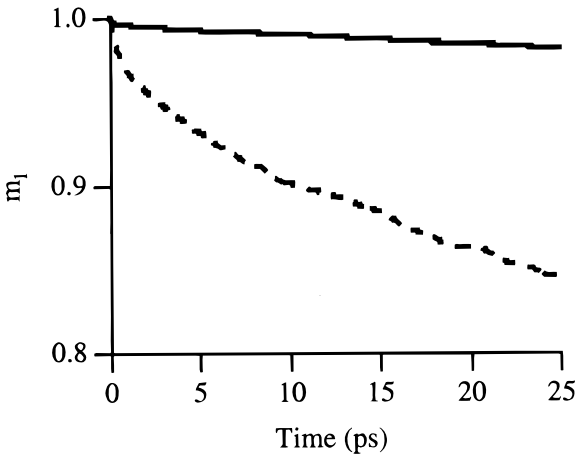

Figure 8. Rotational time correlation function, m_1, for a representative vector, ϕ_3, in the isolated chain (solid line) and the interfacial chain (broken line).

Torsional mobility is determined by not only the rotational energy barriers but also the free volume required to accomplish the rotation. For example, theoretical work has suggested that in the rigid pyromellitimide anhydride rotation about meta linkages requires more free volume than rotation about a para linkage.[38] This is consistent with experimental work showing that meta-linked PMDA/ODA has a lower extent of imidization than its para counterpart.[39,40] For the LaRC-IA polyimide of interest here, both meta- and para-linked sites were equally likely to react. There was no preference for one or the other to react in either stage of imidization. The increased flexibility of the LaRC-IA PAA compared to PMDA/ODA apparently makes LaRC-IA less sensitive to the type of linkage.

The overall PAA chain shape also determines the amount of free volume required for transitions to occur. If the PAA is in an extended conformation, backbone transitions and therefore imidization can occur with minimal disruption to the remainder of the chain. Yoon et al.[41] speculated that local motion (rather than large-scale chain motion) was responsible for imidization when they observed that PMDA/ODA began imidizing well below its glass transition temperature. They attributed this to the extended nature of the PAA monomer as it formed a liquid-crystal-like state. In the LaRC-IA/silica system, the presence of the substrate may also cause the chain to adopt an extended structure. Recall that in an earlier section it was shown that the interfacial chains were more extended than their isolated counterparts. If large-scale chain motions were necessary for imidization, one would expect to see a decrease in the extent of imidization near the substrate because the substrate eliminates one degree of freedom. The high extent of interfacial imidization and increased torsional mobility seen in these simulations, coupled with the previously cited experimental evidence, indi-

Table 5. Percentage of Reactions That Occur without Any Torsional Transition as a Function of the Degree of Imidization

	0−25% imidization	25%−50% imidization	50%−75% imidization	75%−100% imidization
$T = 400$ K, isolated chain	100	100		
$T = 700$ K, isolated chain	80	73	53	33
$T = 400$ K, interfacial chain	54	54	43	
$T = 700$ K, interfacial chain	80	33	7	8

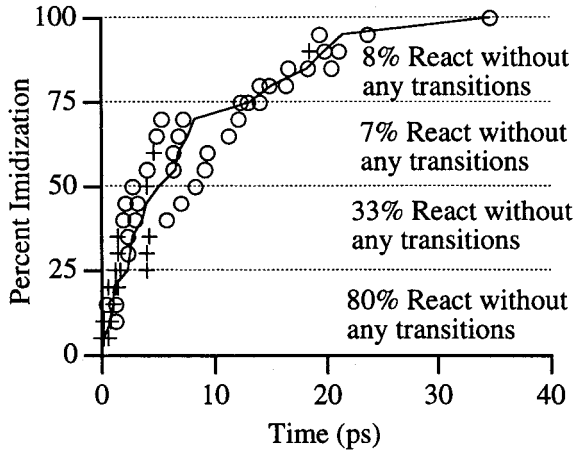

Figure 9. Imidization profile of interfacial chain at $T = 700$ K. (+) denotes reactions in which no torsional transition prior to imidization occurs, (○) denotes reactions that are preceded by torsional transitions, and (—) denotes the average extent of imidization.

cate that imidization proceeds by local mobility rather than large-scale chain rearrangement.

Figure 9 reveals that for the interfacial system at 700 K imidization is initially dominated by reactions in which no torsional transitions occur, while later in the simulation, conformational transitions between states becomes necessary for imidization. Table 5 shows that this trend occurs in all systems. These observations support the physical reasoning set forth by the kinetic models to explain the two stages of imidization: an initial stage controlled by the chemical conversion of functional groups already in the proper conformation for imidization and a subsequent slower stage dominated by reactions in which the groups undergo transitions between conformational states. Although the present model has not incorporated a chemical activation energy, the only effect of doing so would be to change the time scale over which imidization occurs. The particular polyimide studied, LaRC-IA, is very flexible. Therefore, it is probably the decrease in the number of unreacted sites instead of the increase in chain stiffness resulting from imidization which leads to the decreasing rate of imidization.

Conclusions

A novel computational method that allows the mapping of the chemical reaction of imidization into a molecular dynamics simulation has been presented. Specifically, the imidization of the LaRC-IA polyimide in the proximity of the (111) surface of cristobalite silica was examined. Calculations on isolated chains were conducted for comparison. This work provides atomistic evidence that substantiates two theories in polyimide literature. The physical rationale behind the two-stage kinetic models of imidization is substantiated by these calculations. The initial stage of imidization is characterized by the reaction of functional groups already in the proper conformation for imidization, and the second stage is controlled by the ability of functional groups to move between nonequivalent conformational states. Finally, these simulations indicate that local chain motion instead of large-scale chain rearrangement is responsible for the imidization of interfacial chains.

These simulation methods lay the groundwork for the development of more complex models to address the many issues arising in thermal solid-state imidization. Other polyimide systems with varying degrees of flexibility in both the dianhydride and diamine sections and chemisorption between the polymer and substrate are areas of further research. The information gained from these simulations may help guide the development of industrially relevant polyimide interfacial systems.

Acknowledgment. The authors are grateful to the NASA Graduate Students Research Program (NGT-1-52100) and NASA Langley (NAG 11723) for financial support of this work.

References and Notes

(1) vanZanten, J. H.; Wallace, W. E.; Wu, W. L. *Phys. Rev. E* **1996**, *53*, R2053−R2056.
(2) Coburn, J. C.; Pottiger, M. T. In *Polyimides Fundamentals and Applications*; Ghosh, M. K., Mittal, K. L., Eds.; Marcel Dekker: New York, 1996; p 207.
(3) Okamoto, K. In *Polyimides Fundamentals and Applications*; Ghosh, M. K., Mittal, K. L., Eds.; Marcel Dekker: New York, 1996; p 265.
(4) Lim, B. S.; Nowick, A. S.; Lee, K. W.; Viehbeck, A. *J. Polym. Sci., Part B: Polym. Phys.* **1993**, *31*, 545−555.
(5) Hasegawa, M.; Matano, T.; Shindo, Y.; Sugimura, T. *Macromolecules* **1996**, *29*, 7897−7907.
(6) Sanchez, I. C. *Physics of Polymer Surfaces and Interfaces*; Butterworth-Heinemann: Boston, 1992.
(7) Zubkov, V. A. In *Polyamic Acids and Polyimides: Synthesis, Transformations and Structure*; Bessonov, M. I., Zubkov, V. A., Eds.; CRC Press: Ann Arbor, MI, 1993; p 107.
(8) Seo, Y. S. *Polym. Eng. Sci.* **1997**, *37*, 772−776.
(9) Mansfield, K. F.; Theodorou, D. N. *Macromolecules* **1989**, 22, 3143−3152.
(10) Kumar, S. K.; Vacatello, M.; Yoon, D. Y. *J. Chem. Phys.* **1988**, *89*, 5206−5215.
(11) Matsuda, T.; Smith, G. D.; Winkler, R. G.; Yoon, D. Y. *Macromolecules* **1995**, *28*, 165−173.
(12) Winkler, R. G.; Gerstmair, A.; Reineker, P.; Matsuda, T.; Yoon, D. Y. *Int. J. Quantum Chem.* **1994**, *52*, 437−456.
(13) Bitsanis, I.; Hadziioannou, G. *J. Chem. Phys.* **1990**, *92*, 3827−3847.
(14) Bash, P. A.; Ho, L. L.; Mackerell, A. D.; Levine, D.; Hallstrom, P. *Proc. Natl. Acad. Sci. U.S.A.* **1996**, *93*, 3698−3703.
(15) Warshel, A. *Computer Modeling of Chemical Reactions in Enzymes and Solutions*; Wiley: New York, 1991.
(16) Maple, J. R.; Hwang, M. J.; Stockfisch, T. P.; Dinur, U.; Waldman, M.; Ewig, C. S.; Halger, A. T. *J. Comput. Chem.* **1994**, *15*, 162−182.
(17) Jorgensen, W. L.; Swenson, C. J. *J. Am. Chem. Soc.* **1985**, *107*, 569−578.
(18) Rutledge, G. C.; Suter, U. W. *Macromolecules* **1991**, *24*, 1921−1933.
(19) Lautenschlager, P.; Brickmann, J.; Vanruiten, J.; Meier, R. J. *Macromolecules* **1991**, *24*, 1284−1292.
(20) Stewart, J. J. P. MOPAC QCPE Program Number 455.
(21) Laius, L. A.; Tsapovetsky, M. I. In *Polyamic Acids and Polyimides Synthesis, Transformations and Structure*; Bessonov, M. I., Zubkov, V. A., Eds.; CRC Press: Ann Arbor, MI, 1993; p 47.
(22) Bessonov, M. I. *Polyimides: Thermally Stable Polymers*; Plenum Press: New York, 1987.
(23) Bessonov, M. I. *Poliimidy-Klass Termostoykikh Polimerov*; "Nauka" Press: Leningrad, 1983; Vol. A70-42625 UDC 547.639.
(24) Frost, L. W.; Keese, I. *J. Appl. Polym. Sci.* **1964**, *8*, 1039−1051.
(25) Parks, G. A. *Chem. Rev.* **1965**, *65*, 177−198.
(26) Iacona, F.; Garilli, M.; Marletta, G.; Puglisi, O.; Pignataro, S. *J. Mater. Res.* **1991**, *6*, 861−870.
(27) Perry, S. S.; Campion, A. *Surf. Sci.* **1991**, *259*, 207−214.
(28) Sauer, J.; Ugliengo, P.; Garrone, E.; Saunders, V. R. *Chem. Rev.* **1994**, *94*, 2095−2160.
(29) Ugliengo, P.; Ferrari, A. M.; Zecchina, A.; Garrone, E. *J. Phys. Chem.* **1996,** *100*, 3632−3645.
(30) Ugliengo, P.; Bleiber, A.; Garrone, E.; Sauer, J.; Ferrari, A. M. *Chem. Phys. Lett.* **1992**, *191*, 537−547.
(31) Hill, J. R.; Sauer, J. *J. Phys. Chem.* **1994**, *98*, 1238−1244.

(32) Hentschke, R.; Schurmann, B. L.; Rabe, J. P. *J. Chem. Phys.* **1992**, *96*, 6213−6221.
(33) Pelmenschikov, A. G.; Morosi, G.; Gamba, A. *J. Phys. Chem. A* **1997**, *101*, 1178−1187.
(34) Leggetter, S.; Tildesley, D. J. *Mol. Phys.* **1989**, *68*, 519−546.
(35) Harris, F. W. In *Polyimides*; Wilson, D., Stenzenberger, H. D., Hergenrother, P. M., Eds.; Blackie: Glasgow, 1990; p 1.
(36) Jones, R. L.; Kumar, S. K.; Ho, D. L.; Briber, R. M.; Russell, T. P. *Nature* **1999**, *400*, 146−149.
(37) Tsai, W. H.; Cave, N. G.; Boerio, F. J. *Langmuir* **1992**, *8*, 927−935.
(38) Milevskaya, I. S.; Lukasheva, N. V.; Yel'Yashevich, A. M. *Polym. Sci. U.S.S.R.* **1979**, *21*, 1427−1432.
(39) Konieczny, M.; Xu, H. Z.; Battaglia, R.; Wunder, S. L.; Volksen, W. *Polymer* **1997**, *38*, 2969−2979.
(40) Johnson, C.; Wunder, S. L. *J. Polym. Sci., Part B: Polym. Phys.* **1993,** *31***,** 677−692.
(41) Takahashi, N.; Yoon, D. Y.; Parrish, W. *Macromolecules* **1984**, *17*, 2583−2588.
(42) Suzuki, T.; Hirano, M.; Tamon, H.; Okazaki, M. *J. Phys. Chem.* **1995**, *99*, 15968−15972.

MA991639U